

Spin quantum Hall transition on random networks: exact critical exponents via quantum gravity

Esteban Macías,^{1,*} Ilya Gruzberg,^{2,†} and Eldad Bettelheim^{1,‡}

¹*Racah Institute of Physics, Hebrew University of Jerusalem, Jerusalem, 91904, Israel*

²*Department of Physics, Ohio State University, Columbus, Ohio, 43210, USA*

(Dated: February 2, 2026)

We solve the problem of the spin quantum Hall transition on random networks using a mapping to classical percolation that focuses on the boundary of percolating clusters. Using tools of two-dimensional quantum gravity, we compute critical exponents that characterize this transition and confirm that these are related to the exponents for the regular (square) network through the KPZ relation. Our results demonstrate the relevance of the geometric randomness of the networks and support conclusions of numerical simulations of random networks for the integer quantum Hall transition.

Introduction. The integer quantum Hall (IQH) transition is a paradigmatic example of a continuous quantum critical point whose very existence is due to quenched disorder. The universal critical phenomena near such transitions have attracted vigorous interest over the years [1]. Experiments [2–11] demonstrate universal scaling near the IQH transition. The transition is usually modeled as an Anderson transition [1], neglecting electron-electron interactions. There are QH transitions in other symmetry classes of disordered systems [12, 13]. Superconductors with broken time-reversal invariance in 2D can exhibit QH transitions where the spin (class C) [14, 15] or thermal (class D) [16] conductivity of quasiparticles jumps in quantized units.

An intriguing aspect of QH transitions (and other disordered critical points) is the multifractal (MF) scaling of critical electronic wave functions and powers of the local density of states characterized by a continuum of scaling exponents Δ_q , the so-called MF spectrum [1]. More complicated scaling observables lead to generalized MF spectra labeled by multi-component indices [17–26]. The MF spectra are modified near system’s boundaries [27, 28].

Much intuition about the IQH transition, as well as the most accurate numerical estimates for critical exponents, come from the Chalker-Coddington (CC) network model [29, 30] based on the semiclassical picture of electrons drifting along the equipotential lines of a smooth disorder potential. Tunneling across saddle points of the potential leads to delocalization at a critical point. In the CC model this picture is drastically simplified, and all saddle points are modeled as scattering nodes placed at the vertices of a square lattice.

This simplification was challenged in Ref. [31], where it was argued that the CC model does not capture all types of disorder relevant at the IQH transition. Indeed,

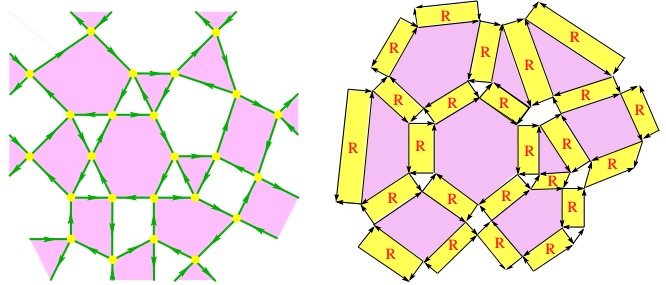


FIG. 1. A random network and its Manhattan lattice

the saddle points that connect the “puddles” of filled electron states do not form a regular lattice, and around each “puddle” there may be any number of them [32, 33]. Taking this into account leads to structurally disordered or *random networks* (RNs) such as the one shown on the left in Fig. 1. The geometric disorder of the network, which has to be treated as quenched and summed over, may be regarded as the inclusion of two-dimensional quantum gravity (2DQG), which changes the universality class of the problem. Numerical studies of variants of random networks [31–35] confirmed this picture [36].

2DQG modifies critical exponents of a statistical model at its critical point placed on a random graph in the way given by the Knizhnik-Polyakov-Zamolodchikov (KPZ) relation [37–39]. The relation has been verified by explicit solutions of critical statistical models defined on random graphs [40–43]. For critical points described by a conformal field theory (CFT) with the central charge $c = 0$ (which should hold for a CFT description of Anderson transitions) the relation is

$$\Delta^{(0)} = \Delta(\Delta + 1)/3, \quad (1)$$

where $\Delta^{(0)}(\Delta)$ are scaling dimensions of operators on a flat (fluctuating) surface.

Ref. [31] proposed to check the KPZ relation (1) by considering other QH transitions. Both SQH and TQH are simpler than the IQH; many of their properties can be determined from mappings to classical models. The

* esteban.macias@mail.huji.ac.il

† gruzberg.1@osu.edu

‡ eldad.bettelheim@mail.huji.ac.il

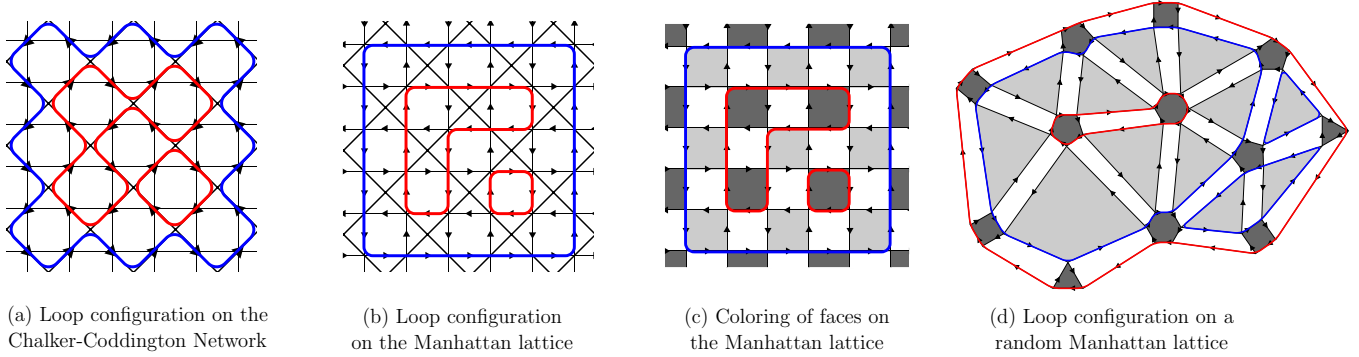


FIG. 2. Loop configurations on flat and random networks.

SQH on the CC network was mapped to classical bond percolation on a square lattice [44, 45]. Exact results known for classical percolation lead to many exact critical properties at the SQH transition [23, 27, 28, 44–48]. The mapping was extended to network models in class C on arbitrary graphs [49, 50], and works for RNs as well.

In this paper, we use the relation of the *critical* bond percolation to the dense phase of the $O(n)$ loop model in the limit $n = 1$, which is achieved by focusing on the un-oriented loops surrounding the percolation clusters (the percolation hulls). These loops densely fill a Manhattan lattice (ML), which is the medial graph of the CC network. Here we provide an exact solution of the $O(n)$ model on random MLs, such as the one shown on the right in Fig. 1, using tools of 2DQG.

We follow the approach based on the loop equations (LEs) [51], recursive relations for partition and correlation functions defined on large random graphs τ (equivalently, discretized surfaces) with the topology of a disk. The LEs result from the ability to cut a given surface into independent parts whose contributions factorize, and then summing over all possible ways of cutting. This approach led to exact critical properties of the $O(n)$ model on random triangulated surfaces [52–55]. Results include the so-called string susceptibility exponent γ describing the scaling of the partition function with the area of the surface, and the boundary ($\tilde{\Delta}_L$) and bulk (Δ_L) dimensions of the so-called L -leg operators (also called the “watermelon exponents”) characterizing the power-law decay of probabilities of multiple loops approaching a point.

We confirm the universal nature of γ , $\tilde{\Delta}_L$, and Δ_L by deriving them from the LEs adapted to arbitrary random MLs, see Eqs. (14), (21), and (23). The KPZ relation (1) maps the QG scaling dimensions $\tilde{\Delta}_L$ and Δ_L to their counterparts in regular geometry that turn out to be the known percolation scaling dimensions (22), (24). In our context, this confirms the relevance of the random geometry at the regular SQH transition, and lends more credibility to numerical results of Refs. [31–35]. Also, the multi-leg dimensions Δ_L give some MF exponents [23], that, therefore, satisfy the KPZ scaling relation (1).

By universality, we expect the KPZ relation to apply to other critical exponents. A companion paper [56] uses the relation of classical percolation to the q -states Potts model in the limit $q = 1$, and directly computes the thermodynamic critical exponent α and the 2DQG analog of the localization length exponent ν that describes the scaling of the volume occupied by percolation clusters. These are related to the scaling dimension Δ_t of the thermal operator, and provide an independent verification of the KPZ relation (1) for the SQH transition on RNs.

Disk partition function of random MLs. Loop configurations on the CC network can be mapped to the ML, which is the medial graph of the CC network (see Fig. 2). There are three types of faces on the ML: clockwise, counterclockwise, and unoriented, which we color black, gray, and white, respectively (see Fig. 2 (c)). The white faces correspond to the scattering nodes of the CC network.

A random ML is obtained by allowing oriented faces to be arbitrary polygons but keeping the unoriented faces as quadrilaterals. To preserve the structure of the network, we forbid oppositely oriented faces from sharing sides, and faces with the same orientation from sharing corners. We color these faces the same way as for the square CC network in Fig. 2. An example of a random ML is shown in Fig. 2 (d).

We impose reflecting boundary conditions (that is, when a loop reaches the boundary, it is reflected with probability 1) by placing an additional loop that frames the surface but does not contribute to the partition function. As a consequence, the number of sides of a colored face that are part of the boundary is arbitrary. Thus, our convention is to maximally reduce the number of boundary sides, see Fig. 3. Then we define the length l of the boundary as the number of sides of oriented (black or gray) polygons along the boundary once they have been maximally reduced. For example, the length of the boundary of the surface in Fig. 2 (d) is 8.

We only consider planar surfaces τ with one boundary component, that is, those with the Euler characteristic $\chi(\tau) = 1$. Then the framing loops provide clockwise or counterclockwise orientation to the surfaces. The area

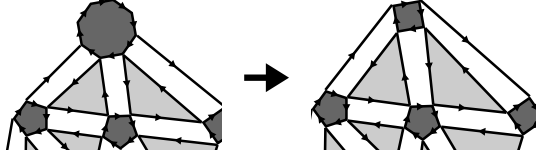


FIG. 3. A colored piece on the boundary of a clockwise oriented random ML (left) and the equivalent boundary with convention mentioned in the text (right).

$A(\tau)$ of a surface τ is defined as the number of white faces of τ . The disk partition function is the sum over surfaces with a fixed (say, clockwise) orientation and over loop configurations on them:

$$\Phi(x, \zeta) = \sum_{\tau} \frac{x^{-A(\tau)} \zeta^{-l(\tau)}}{l(\tau)} \sum_{\text{loops} \in \tau} n^{\#\text{loops}}, \quad (2)$$

where x , ζ , and n are fugacities associated with the area $A(\tau)$, the boundary length $l(\tau)$, and the number of loops. We also consider the partition function for surfaces with a marked point (a colored side) on the boundary:

$$W(x, \zeta) = -\partial_{\zeta} \Phi(x, \zeta) = \sum_{l=0}^{\infty} \zeta^{-l-1} W_l(x), \quad (3)$$

which serves as a generating function for partition functions W_l for surfaces with a fixed boundary length l .

The partition functions for counterclockwise oriented surfaces are denoted as $\dot{\Phi}$, \dot{W} , etc. The values of W_l and \dot{W}_l are the same, as the contributing surfaces and loop configurations are in a one-to-one correspondence, and we use the single fugacity ζ for both orientations. Nevertheless, as we will see, it is useful to keep the distinction to determine the location of the critical point.

Critical behavior. The fugacities x and ζ have critical values, x_c and ζ_c , near which the partition functions Φ and W exhibit critical behavior. Near criticality, when $\delta x = x - x_c \ll 1$, $\delta \zeta = \zeta - \zeta_c \ll 1$, the average area and boundary length of random surfaces diverge as

$$\langle A \rangle = -x \partial_x \ln \Phi(x, \zeta) \sim \delta x^{-1}, \quad (4)$$

$$\langle l \rangle_{x=x_c} = -\zeta \partial_{\zeta} \ln \Phi(x, \zeta)|_{x=x_c} \sim \delta \zeta^{-1}. \quad (5)$$

Critical exponents of interest to us include the string susceptibility exponent γ which describes the singular behavior of Φ :

$$\Phi(x, \zeta_c) \sim \delta x^{1-\frac{\gamma}{2}}, \quad (6)$$

and the exponent ν_l describing the singularity of the average boundary length:

$$\langle l \rangle_{\zeta=\zeta_c} = -\zeta \partial_{\zeta} \ln \Phi(x, \zeta)|_{\zeta=\zeta_c} \sim \delta x^{-\frac{1}{2\nu_l}}. \quad (7)$$

Combining this with Eq. (5) we get the scaling form for $\Phi(x, \zeta)$ and $W(x, \zeta)$ near the critical point (x_c, ζ_c) :

$$\Phi(x, \zeta) \sim \delta x^{1-\frac{\gamma}{2}} \phi(s), \quad s = \delta x^{\frac{1}{2\nu_l}} / \delta \zeta, \quad (8)$$

$$W(x, \zeta) \sim \delta x^{1-\frac{\gamma}{2}-\frac{1}{2\nu_l}} s^2 \phi'(s), \quad (9)$$

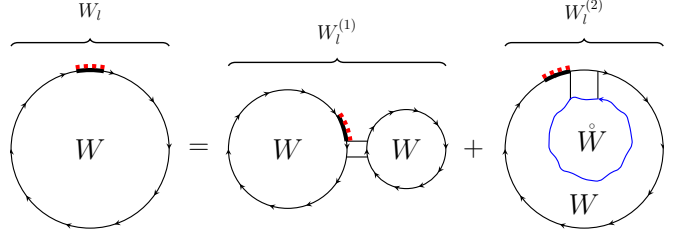


FIG. 4. Two ways of splitting a surface.

where the scaling function $\phi(s)$ has the asymptotics

$$\phi(s) \sim \begin{cases} s^{\nu_l(\gamma-2)}, & s \rightarrow 0, \\ 1 + C s^{-1}, & s \rightarrow \infty. \end{cases} \quad (10)$$

When one of the fugacities takes its critical value, we obtain

$$W(x, \zeta_c) \sim \delta x^{1-\frac{\gamma}{2}-\frac{1}{2\nu_l}}, \quad W(x_c, \zeta) \sim \delta \zeta^{\nu_l(2-\gamma)-1}. \quad (11)$$

Loop equations for $W(x, \zeta)$ follow from combinatorial arguments [51–53, 55]. The partition functions W_l satisfy a recursion relation that is derived by splitting the surfaces that contribute to them into two parts such that the weights of the parts factorize. Our splitting procedure is to remove the white face that follows the marked boundary side in the direction of the framing loop. This can split surfaces in two possible ways: $W_l = W_l^{(1)} + W_l^{(2)}$, see Fig. 4. In the first case, the white face is not adjacent to an inner loop, and its removal breaks the surface into two parts with the same orientation (see Fig. 5 (a)). In the second case the white face is adjacent to an inner loop, and after its removal the inner loop is partially exposed. Cutting along this inner loop splits the surface into two oppositely oriented surfaces. An example of this is shown in Fig. 5 (b). In both cases there are eight distinct subcases, see Appendix A for details.

Combining all possible ways of splitting a surface with the definition (3) gives a functional LE for the generating function (the argument x is suppressed for brevity):

$$W(\zeta) = f_0(\zeta) + f_1(\zeta)W(\zeta) + \frac{(1+\zeta)^3}{x\zeta} W^2(\zeta) + n \frac{1+\zeta}{x\zeta^2} \oint \frac{dz}{2\pi iz} \frac{(1+z)^2 W(z) \dot{W}(1/z)}{\zeta - z}. \quad (12)$$

As we show in the Appendix A, the functions $f_{0,1}$ are less singular near the critical point than W and are not important for finding critical exponents. The singular behavior of W is determined by the ratio of the coefficients of the two bilinear terms in Eq. (12) near criticality. The second of these (stemming from $W_l^{(2)}$) contains $W(\zeta)$ and $\dot{W}(1/\zeta)$. This determines the critical value $\zeta_c = 1$. At this point the two oppositely oriented surfaces have the same boundary fugacity, which is what we expect in the critical Potts model.

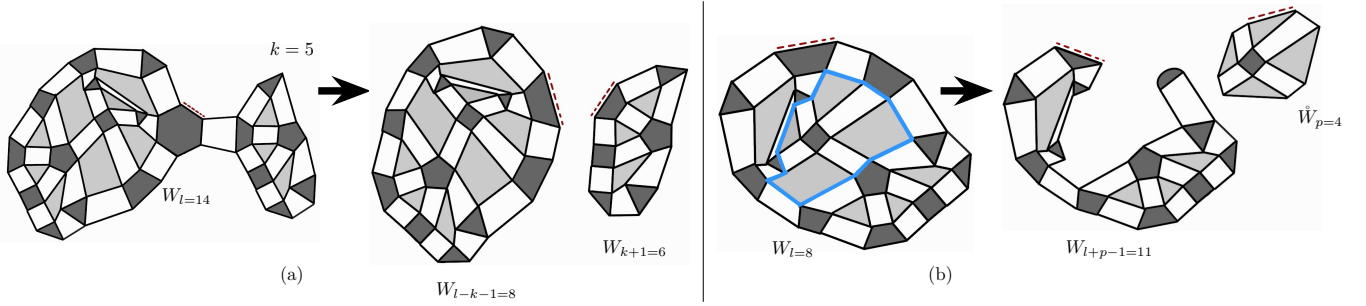


FIG. 5. Examples of a clockwise oriented surface split in two ways by removing the white face adjacent to the marked black boundary side. (a) The removal of the white face immediately gives two separate surfaces. This splitting contributes to $W_l^{(1)}$ in Fig. 4. (b) The removal of the white face follows cutting along the exposed inner loop (in blue). The rightmost surface gives another example of our boundary drawing convention, where we maximally reduce boundary sides of colored polygons.

Analysis of Eq. 12 (see Appendix A) gives

$$W(x_c, \zeta) \sim \delta \zeta^{2/3}, \quad W(x, \zeta_c) \sim \delta x^{1/2}. \quad (13)$$

Comparing with Eq. (11) we obtain the exponents

$$\gamma = -1/2, \quad \nu_l = 2/3. \quad (14)$$

L-leg operators. Another family of exponents of interest are the boundary scaling dimensions $\tilde{\Delta}_L$, which are obtained by analyzing the critical behavior of the two point functions of the L -leg operators. These are defined by marking two points on the boundary of each surface, inserting L mutually and self-avoiding lines (legs) $\{\gamma^{(i)}\}_{i=1}^L$ connecting them, and considering loop configurations that avoid the edges occupied by the L legs.

For fixed boundary lengths l and l' between the marked points, the (unnormalized) two point function is given by

$$D_{ll'}^L = \sum_{\tau_{ll'}} x^{-A(\tau_{ll'})} \sum_{\{\gamma^{(i)}\}} \sum_{\text{loops} \in \tau_{ll'} / \cup_i \gamma^{(i)}} n^{\#\text{loops}}, \quad (15)$$

The corresponding generating function is

$$D^L(x, \zeta) = \sum_{ll'} \zeta^{-l-1} \zeta^{-l'-1} D_{ll'}^L. \quad (16)$$

The boundary dimensions $\tilde{\Delta}_L$ enter the critical scaling of $D^L(x, \zeta)$ (See Eqs. (B.54) and (B.56) in [54]) as

$$D^L(x, \zeta_c) \sim \delta x^{\frac{\tilde{\Delta}_L}{2}-1} \delta \zeta^{1-\frac{\gamma}{2}}, \quad (17)$$

$$D^L(x_c, \zeta) \sim \delta \zeta^{\nu_l(\tilde{\Delta}_L-2)} \delta \zeta^{\nu_l(2-\gamma)}. \quad (18)$$

The factors involving ν_l and γ are due to the fact that we did not normalize the correlation function.

Similarly to the derivation of the LE for W , the surfaces that contribute to D^L can be decomposed by successively cutting along the L legs, see Appendix (B). The decomposition can be used recursively to show that

$$D^L(x_c, \zeta) \sim \delta \zeta^{-1} W^{\lfloor L/2 \rfloor + 1}(\zeta) \hat{W}^{\lceil L/2 \rceil}(1/\zeta). \quad (19)$$

Regardless of the parity of L , when ζ is close to its critical value, the scaling (13) implies

$$D^L \sim \delta \zeta^{(2L-1)/3}, \quad (20)$$

which gives the boundary dimensions

$$\tilde{\Delta}_L = L - 1. \quad (21)$$

Using the KPZ map (1) we get

$$\tilde{\Delta}_L^{(0)} = L(L-1)/3, \quad (22)$$

which are the known boundary scaling dimensions of percolation in the plane.

The boundary dimensions in QG are related to the bulk dimensions by $\tilde{\Delta}_L = 2\Delta_L$ [54]. This relation yields

$$\Delta_L = (L-1)/2. \quad (23)$$

Again, the KPZ map (1) gives

$$\Delta_L^{(0)} = (L^2 - 1)/12, \quad (24)$$

the known bulk dimensions of L -leg operators for percolation in the plane. This result again confirms the validity of the KPZ map.

Discussion. In conclusion, we have solved the problem of the spin quantum Hall transition on random networks by considering an alternative form of the percolation mapping for the transition that focuses on boundaries of percolating clusters. We extended the mapping to random networks and computed exact critical exponents that characterize the transition. Thereby, we confirmed the validity of the KPZ formula that relates the critical exponents on random networks to the known exponents for percolation in the plane.

Our results provide support for the findings of Refs. [31–35], which showed that random modifications of the Chalker-Coddington network model change critical exponents at the integer quantum Hall transition.

Looking ahead, we believe that methods using two-dimensional quantum gravity can be extended to better

understand the IQH transition. In particular, Ref. [57] introduced a procedure in which the IQH transition is viewed as the limit of a sequence of statistical models, which we believe can be solved exactly through appropriate extensions of methods used in this paper. We plan to address this problem in the future.

ACKNOWLEDGMENTS

This research was supported by Grant No. 2020193 from the United States-Israel Binational Science Foun-

dation (BSF). IG acknowledges V. A. Kazakov and A. Mukherjee for discussions and a collaboration on a closely-related project [56].

[1] F. Evers and A. D. Mirlin, Anderson transitions, *Rev. Mod. Phys.* **80**, 1355 (2008).

[2] H. P. Wei, D. C. Tsui, M. A. Paalanen, and A. M. M. Pruisken, Experiments on delocalization and universality in the integral quantum Hall effect, *Phys. Rev. Lett.* **61**, 1294 (1988).

[3] S. Koch, R. J. Haug, K. v. Klitzing, and K. Ploog, Experiments on scaling in $\text{Al}_x\text{Ga}_{1-x}\text{As}/\text{GaAs}$ heterostructures under quantum Hall conditions, *Phys. Rev. B* **43**, 6828 (1991).

[4] S. Koch, R. J. Haug, K. v. Klitzing, and K. Ploog, Size-dependent analysis of the metal-insulator transition in the integral quantum Hall effect, *Phys. Rev. Lett.* **67**, 883 (1991).

[5] S. Koch, R. J. Haug, K. v. Klitzing, and K. Ploog, Experimental studies of the localization transition in the quantum Hall regime, *Phys. Rev. B* **46**, 1596 (1992).

[6] L. W. Engel, D. Shahar, C. Kurdak, and D. C. Tsui, Microwave frequency dependence of integer quantum Hall effect: Evidence for finite-frequency scaling, *Phys. Rev. Lett.* **71**, 2638 (1993).

[7] H. P. Wei, L. W. Engel, and D. C. Tsui, Current scaling in the integer quantum Hall effect, *Phys. Rev. B* **50**, 14609 (1994).

[8] W. Li, G. A. Csáthy, D. C. Tsui, L. N. Pfeiffer, and K. W. West, Scaling and universality of integer quantum Hall plateau-to-plateau transitions, *Phys. Rev. Lett.* **94**, 206807 (2005).

[9] W. Li, C. L. Vicente, J. S. Xia, W. Pan, D. C. Tsui, L. N. Pfeiffer, and K. W. West, Scaling in plateau-to-plateau transition: A direct connection of quantum Hall systems with the anderson localization model, *Phys. Rev. Lett.* **102**, 216801 (2009).

[10] A. J. M. Giesbers, U. Zeitler, L. A. Ponomarenko, R. Yang, K. S. Novoselov, A. K. Geim, and J. C. Maan, Scaling of the quantum Hall plateau-plateau transition in graphene, *Phys. Rev. B* **80**, 241411 (2009).

[11] S. Kaur, T. Chanda, K. R. Amin, D. Sahani, K. Watanabe, T. Taniguchi, U. Ghorai, Y. Gefen, G. J. Sreejith, and A. Bid, Universality of quantum phase transitions in the integer and fractional quantum Hall regimes, *Nature Communications* **15**, 8535 (2024), arXiv:2312.06194 [cond-mat.mes-hall].

[12] M. R. Zirnbauer, Riemannian symmetric superspaces and their origin in random-matrix theory, *J. Math. Phys.* **37**, 4986 (1996).

[13] A. Altland and M. R. Zirnbauer, Nonstandard symmetry classes in mesoscopic normal-superconducting hybrid structures, *Phys. Rev. B* **55**, 1142 (1997).

[14] V. Kagalovsky, B. Horovitz, Y. Avishai, and J. T. Chalker, Quantum Hall Plateau Transitions in Disordered Superconductors, *Physical Review Letters* **82**, 3516 (1999).

[15] T. Senthil, J. B. Marston, and M. P. A. Fisher, Spin quantum Hall effect in unconventional superconductors, *Phys. Rev. B* **60**, 4245 (1999).

[16] T. Senthil and M. P. A. Fisher, Quasiparticle localization in superconductors with spin-orbit scattering, *Phys. Rev. B* **61**, 9690 (2000).

[17] D. Höf and F. Wegner, Calculation of anomalous dimensions for the nonlinear sigma model, *Nuclear Physics B* **275**, 561 (1986).

[18] F. Wegner, Anomalous dimensions for the nonlinear sigma-model in $2 + \varepsilon$ dimensions (I), *Nuclear Physics B* **280**, 193 (1987).

[19] F. Wegner, Anomalous dimensions for the nonlinear sigma-model, in $2 + \varepsilon$ dimensions (II), *Nuclear Physics B* **280**, 210 (1987).

[20] I. A. Gruzberg, A. W. W. Ludwig, A. D. Mirlin, and M. R. Zirnbauer, Symmetries of multifractal spectra and field theories of Anderson localization, *Phys. Rev. Lett.* **107**, 086403 (2011).

[21] I. A. Gruzberg, A. D. Mirlin, and M. R. Zirnbauer, Classification and symmetry properties of scaling dimensions at Anderson transitions, *Phys. Rev. B* **87**, 125144 (2013).

[22] J. F. Karcher, N. Charles, I. A. Gruzberg, and A. D. Mirlin, Generalized multifractality at spin quantum Hall transition, *Annals of Physics* **435**, 168584 (2021), arXiv:2107.06414 [cond-mat.dis-nn].

[23] J. F. Karcher, I. A. Gruzberg, and A. D. Mirlin, Generalized multifractality at the spin quantum Hall transition: Percolation mapping and pure-scaling observables, *Phys. Rev. B* **105**, 184205 (2022), arXiv:2203.12617 [cond-mat.dis-nn].

[24] J. F. Karcher, I. A. Gruzberg, and A. D. Mirlin, Generalized multifractality at metal-insulator transitions and in metallic phases of two-dimensional disordered systems, *Phys. Rev. B* **106**, 104202 (2022), arXiv:2206.12226 [cond-mat.dis-nn].

[25] J. F. Karcher, I. A. Gruzberg, and A. D. Mirlin, Gener-

alized multifractality in two-dimensional disordered systems of chiral symmetry classes, *Phys. Rev. B* **107**, 104202 (2023).

[26] J. F. Karcher, I. A. Gruzberg, and A. D. Mirlin, Metal-insulator transition in a two-dimensional system of chiral unitary class, *Phys. Rev. B* **107**, L020201 (2023), arXiv:2210.03131 [cond-mat.dis-nn].

[27] A. R. Subramaniam, I. A. Gruzberg, A. W. W. Ludwig, F. Evers, A. Mildenberger, and A. D. Mirlin, Surface Criticality and Multifractality at Localization Transitions, *Physical Review Letters* **96**, 126802 (2006).

[28] A. R. Subramaniam, I. A. Gruzberg, and A. W. W. Ludwig, Boundary criticality and multifractality at the two-dimensional spin quantum Hall transition, *Phys. Rev. B* **78**, 245105 (2008).

[29] J. T. Chalker and P. D. Coddington, Percolation, quantum tunnelling and the integer Hall effect, *J. Phys. C* **21**, 2665 (1988).

[30] B. Kramer, T. Ohtsuki, and S. Kettemann, Random network models and quantum phase transitions in two dimensions, *Phys. Rep.* **417**, 211 (2005).

[31] Gruzberg, Ilya and Klümper, Andreas and Nuding, Win and Sedrakyan, Ara, Geometrically disordered network models, quenched quantum gravity, and critical behavior at quantum Hall plateau transitions, *Phys. Rev. B* **95**, 125414 (2017), arXiv:1604.06844 [cond-mat.dis-nn].

[32] R. Conti, H. Topchyan, R. Tateo, and A. Sedrakyan, Geometry of random potentials: Induction of two-dimensional gravity in quantum Hall plateau transitions, *Phys. Rev. B* **103**, L041302 (2021).

[33] H. Topchyan, W. Nuding, A. Klümper, and A. Sedrakyan, Harris-Luck criterion in the plateau transition of the integer quantum Hall effect, *Phys. Rev. B* **111**, L100201 (2025), arXiv:2411.01651 [cond-mat.dis-nn].

[34] A. Klümper, W. Nuding, and A. Sedrakyan, Random network models with variable disorder of geometry, *Phys. Rev. B* **100**, 140201 (2019), arXiv:1907.00760 [cond-mat.dis-nn].

[35] H. Topchyan, I. A. Gruzberg, W. Nuding, A. Klümper, and A. Sedrakyan, Integer quantum Hall transition: An S-matrix approach to random networks, *Phys. Rev. B* **110**, L081112 (2024).

[36] Note that the randomness of the network should be treated on the same footing as other types of disorder, which implies that the quantum gravity fluctuations are quenched [?]. While the quenched 2DQG is not solvable for generic values of the central charge c of the critical matter fields, and the KPZ relation may not be valid in this situation, the case of $c = 0$ is special. In this case the quenched and the annealed versions of the 2DQG are equivalent, and the KPZ relation applies. In particular, $c = 0$ for 2D Anderson transitions and percolation.

[37] V. G. Knizhnik, A. M. Polyakov, and A. B. Zamolodchikov, Fractal structure of 2D quantum gravity, *Mod. Phys. Lett. A* **3**, 819 (1988).

[38] F. David, Conformal Field Theories Coupled to 2D Gravity in the Conformal Gauge, *Mod. Phys. Lett. A* **3**, 1651 (1988).

[39] J. Distler and H. Kawai, Conformal Field Theory and 2D Quantum Gravity, *Nucl. Phys. B* **321**, 509 (1989).

[40] V. A. Kazakov, Exactly solvable Potts models, bond- and tree-like percolation on dynamical (random) planar lattice, *Nucl. Phys. B Proc. Supp.* **4**, 93 (1988).

[41] V. A. Kazakov and A. A. Migdal, Recent progress in the theory of noncritical strings, *Nucl. Phys. B* **311**, 171 (1988).

[42] V. A. Kazakov, Percolation on a Fractal with the Statistics of Planar Feynman Graphs: Exact Solution, *Mod. Phys. Lett. A* **4**, 1691 (1989).

[43] B. Duplantier and I. K. Kostov, Geometrical critical phenomena on a random surface of arbitrary genus, *Nuclear Physics B* **340**, 491 (1990).

[44] I. A. Gruzberg, A. W. W. Ludwig, and N. Read, Exact Exponents for the Spin Quantum Hall Transition, *Physical Review Letters* **82**, 4524 (1999).

[45] A. D. Mirlin, F. Evers, and A. Mildenberger, Wavefunction statistics and multifractality at the spin quantum Hall transition, *Journal of Physics A Mathematical General* **36**, 3255 (2003).

[46] J. Cardy, Linking Numbers for Self-Avoiding Loops and Percolation: Application to the Spin Quantum Hall Transition, *Physical Review Letters* **84**, 3507 (2000).

[47] R. Bondesan, I. A. Gruzberg, J. L. Jacobsen, H. Obuse, and H. Saleur, Exact Exponents for the Spin Quantum Hall Transition in the Presence of Multiple Edge Channels, *Physical Review Letters* **108**, 126801 (2012).

[48] S. Bhardwaj, I. A. Gruzberg, and V. Kagalovsky, Relevant perturbations at the spin quantum Hall transition, *Phys. Rev. B* **91**, 035435 (2015).

[49] E. J. Beaman, J. Cardy, and J. T. Chalker, Quantum and classical localization, the spin quantum Hall effect, and generalizations, *Phys. Rev. B* **65**, 214301 (2002).

[50] J. Cardy, Network Models in Class C on Arbitrary Graphs, *Comm. Math. Phys.* **258**, 87 (2005).

[51] I. K. Kostov, The ADE face models on a fluctuating planar lattice, *Nuclear Physics B* **326**, 583 (1989).

[52] I. K. Kostov, $O(n)$ vector model on a planar random lattice: spectrum of anomalous dimensions, *Modern Physics Letters A* **4**, 217 (1989).

[53] B. Duplantier and I. K. Kostov, Geometrical critical phenomena on a random surface of arbitrary genus, *Nuclear Physics B* **340**, 491 (1990).

[54] B. Duplantier, Conformal fractal geometry and boundary quantum gravity, arXiv preprint math-ph/0303034 (2003).

[55] I. Kostov, Boundary loop models and 2d quantum gravity, *Journal of Statistical Mechanics: Theory and Experiment* **2007**, P08023 (2007).

[56] A. Mukherjee, I. A. Gruzberg, and V. A. Kazakov, (2026), (in preparation).

[57] Y. Ikhlef, P. Fendley, and J. Cardy, Integrable modification of the critical chalker-coddington network model, *Physical Review B—Condensed Matter and Materials Physics* **84**, 144201 (2011).

Appendix A: Loop equations

In this appendix, we provide some details of the derivation of the loop equations that were glossed over in the main text. There, we described that a random surface can be split in two different ways both of which begin by removing the white face next to a marked black side on the boundary of the surface. This procedure leads to the representation

$$W_l = W_l^{(1)} + W_l^{(2)}, \quad (\text{A1})$$

where each of the two terms can be recursively written as a sum of products of partition functions of the split parts.

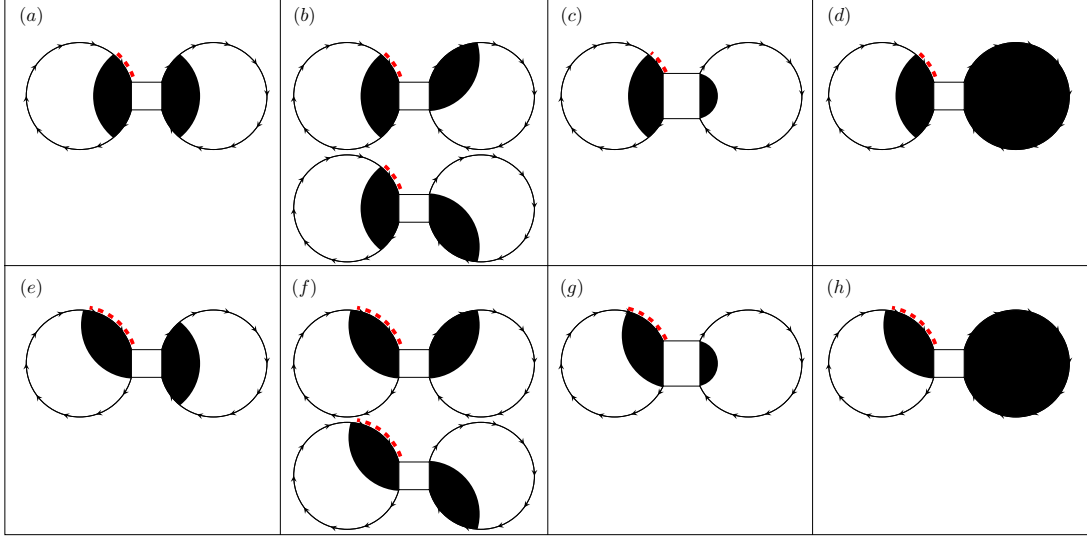


FIG. 6. Here each white circle represents a surface that would result from removing the white square next to the marked boundary side which is indicated by a red dotted line.

In the case of $W_l^{(1)}$, the removal of the white square immediately separates the surface into two parts. To correctly calculate $W_l^{(1)}$ we must include all possible ways in which such a separation can happen. In other words, we need to account for all possible ways two surfaces can be connected by a single white face. We count the total of eight ways in which this can happen, two of which have a combinatorial factor of 2. These eight ways are schematically shown in Fig. (6). Rules for connecting surfaces mostly depend in simple way on the boundary lengths of each part. However, there is an exception to the rule for surfaces with minimal area $A = 0$. Accounting everything, we get the recursion relation for $W_l^{(1)}$:

$$W_l^{(1)} = x^{-1} \left[\sum_{k=2}^{l-2} W_{l-k-1} W_{k-1} H_{l-4} + \sum_{k=1}^{l-2} W_{l-k-1} W_k H_{l-3} + 2 \sum_{k=2}^{l-1} W_{l-k} W_{k-1} H_{l-3} - W_{l-2} H_{l-3} \right. \\ \left. + \sum_{k=0}^{l-2} W_{l-k-1} W_{k+1} H_{l-2} + 2 \sum_{k=1}^{l-1} W_{l-k} W_k H_{l-2} - W_{l-1} H_{l-2} + \sum_{k=0}^{l-1} W_{l-k} W_{k+1} H_{l-1} \right] \quad (\text{A2})$$

where H_n is a discrete step function defined by

$$H_n = \begin{cases} 0 & \text{if } n < 0, \\ 1 & \text{if } n \geq 0. \end{cases} \quad (\text{A3})$$

The third and sixth terms in Eq. (A2) count surfaces that correspond to panels (b) and (d), and (f) and (h), respectively. However, they double count surfaces that correspond to panels (d) and (h), in which the surface to the right consists of a single black face. The fourth and seventh terms correct for this double counting.

In the second type of splitting, after removing the white square, an inner loop is exposed, and this determines how to cut the original surface into two parts. The resulting two surfaces have opposite orientations. Thus, to compute

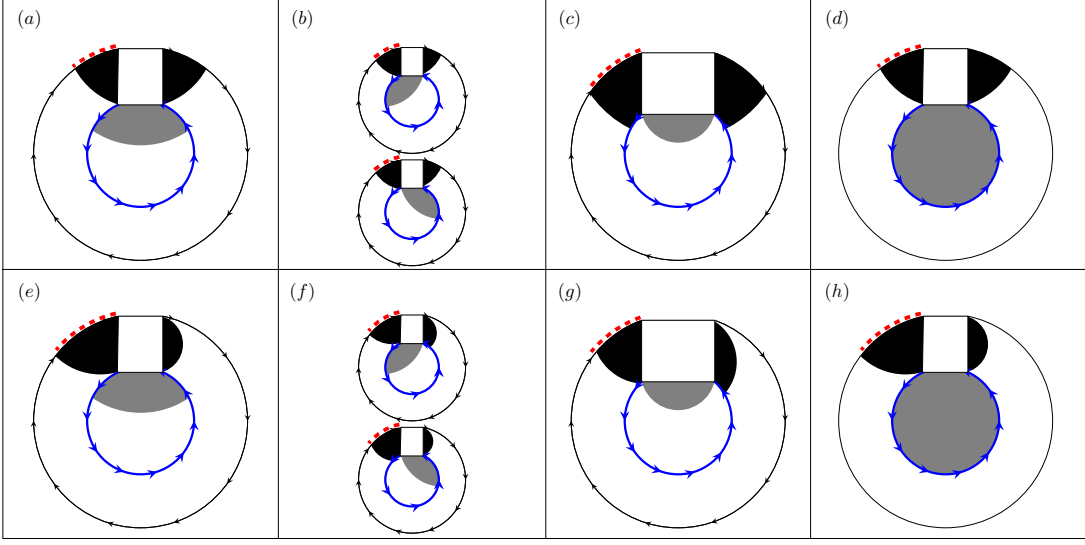


FIG. 7. Here each white circle represents a surface that would result from removing the white square next to the marked boundary side and cutting along the blue loop.

$W_l^{(2)}$, we must include all possible ways to wrap a black square and a white square around a gray surface. There are also eight ways to do this, depending on how the removed white face is connected to the two surfaces. These are shown schematically in Fig. 7 and, in a certain sense, parallel those for $W_l^{(1)}$. Like in the first case, the splittings mostly follow a simple rule that depends on the boundary length of each surface with the exception of the surfaces with minimal area $A = 0$. This gives the second term of Eq. (A1):

$$W_l^{(2)} = x^{-1}n \left[\sum_{p=2}^{\infty} W_{l+p-2} \dot{W}_p H_{l-2} + 2 \sum_{p=2}^{\infty} W_{l+p-1} \dot{W}_p H_{l-2} + \sum_{p=2}^{\infty} W_{l+p-1} \dot{W}_p H_{l-1} + 2 \sum_{p=2}^{\infty} W_{l+p} \dot{W}_p H_{l-1} \right. \\ \left. + \sum_{p=1}^{\infty} W_{l+p} \dot{W}_p H_{l-2} + \sum_{p=1}^{\infty} W_{l+p+1} \dot{W}_p H_{l-1} + (W_l - W_{l+1}) H_{l-2} + (W_{l+1} - W_{l+2}) H_{l-1} \right]. \quad (\text{A4})$$

The fifth and sixth terms in Eq. (A4) are the contributions from surfaces that correspond to panels (a) and (e) of Fig. 7 but also include the weight of a splitting that does not occur for which the eighth and tenth terms correct.

Substituting Eqs. (A2) and (A4) into the definition (3), after rearrangements of the resulting double sums, we obtain Eq. (12) with the non-critical functions f_0 and f_1 given by

$$f_0(x, \zeta) = \frac{1}{\zeta} + \frac{1 + \zeta + (1 + \zeta)^3}{x\zeta^3} + \frac{n(1 + \zeta)[1 + (1 + \zeta)^2 + (1 + 2\zeta)\dot{W}_1 + (2 + \zeta)W_1 + W_2 + 2W_1\dot{W}_1]}{x\zeta^2}, \quad (\text{A5a})$$

$$f_1(x, \zeta) = -\frac{1 + 2\zeta + 2(1 + \zeta)^3}{x\zeta^2} - \frac{n(1 + \zeta)[1 + 2\zeta + \zeta^3 + (1 + 2\zeta)W_1]}{x\zeta^2}. \quad (\text{A5b})$$

Close to the critical point, the LE (12) can be written in terms of the *boundary chemical potential* μ defined by $\zeta = e^\mu$ ($z = e^\lambda$) which gives

$$W(1 + \mu) = f_0(x, 1) + f_1(x, 1)W(1 + \mu) + \frac{8}{x}W^2(1 + \mu) + \frac{8n}{x} \oint_C \frac{d\lambda}{2\pi i} \frac{W(1 + \lambda)\dot{W}(1 - \lambda)}{\mu - \lambda} \quad (\text{A6})$$

where the contour C contains the branch cut of $W(1 + \lambda)$ and excludes the cut of $W(1 - \lambda)$. To get rid of the integral we can change $\mu \rightarrow -\mu$ and $\lambda \rightarrow -\lambda$ in Eq. (A6) and add this transformed version back to Eq. (A6). Adding the contours of integration and using Cauchy's theorem to perform the integral to get

$$W^2(1 + \mu) + W^2(1 - \mu) + nW(1 + \mu)W(1 - \mu) = \frac{x}{8} [(1 - f_1)(W(1 + \mu) + W(1 - \mu)) - 2f_0] \quad (\text{A7})$$

From here the LE can be further simplified by the shift

$$W(1 + \mu) = w(\mu) - \frac{x(f_1(x, 1) - 1)}{8(n + 2)}, \quad (\text{A8})$$

which removes the terms linear in $W(\mu)$ and gives

$$w^2(\mu) + w^2(-\mu) + nw(\mu)w(-\mu) = \frac{x^2(f_1(x, 1) - 1)^2}{64(n + 2)} - \frac{x}{4}f_0(x, 1). \quad (\text{A9})$$

The left hand side of Eq. (A9) vanishes for some value $x = x_c$. For this value the equation can be reduced to

$$w(\mu) = -e^{-i\pi\theta}w(-\mu), \quad (\text{A10})$$

where $n = 2\cos(\pi\theta)$. This uniquely determines the power law behavior for small μ , which is given by the smallest positive power law solution of Eq. (A10). This is given by

$$w(\mu) \sim \mu^{1-\theta}. \quad (\text{A11})$$

Comparison with the scaling form in Eq. (11) gives a relation between critical exponents:

$$\nu_l(2 - \gamma) - 1 = 1 - \theta. \quad (\text{A12})$$

On the other hand setting $\mu = 0$ on Eq. (A9) and expanding in powers of $\delta x = x - x_c$ gives

$$w^2(0, \delta x) = a_1\delta x + a_2\delta x^2 + a_3\hat{W}_1(\delta x) + a_3\delta x\hat{W}_1(\delta x) + a_5\hat{W}_1^2(\delta x) + a_6\hat{W}_2(\delta x), \quad (\text{A13})$$

where \hat{W}_k is the critical part of W_k . The smallest power of δx in Eq. (A13) determines a second exponent equation. To determine this power we must know how the functions \hat{W}_k behave for small δx . This can be done by considering that

$$W_k = \oint_{\infty} \frac{dz}{2\pi i} z^k W(z) \implies \hat{W}_k = \oint_{\infty} \frac{dz}{2\pi i} z^k w(z - 1), \quad (\text{A14})$$

and that this contour integral is dominated by the endpoints of the branch cut $[1 - a, 1]$. Near that region and for small enough δx we can use the scaling form (9), which can be rewritten as

$$w(\delta\zeta, \delta x) \sim \delta\zeta^{\nu_l(2-\gamma)-1}\tilde{\phi}(s), \quad (\text{A15})$$

where the scaling function

$$\tilde{\phi}(s) = s^{\nu_l(2-\gamma)+1}\phi'(s) \sim \begin{cases} 1, & s \ll 1, \\ s^{\nu_l(2-\gamma)-1}, & s \gg 1. \end{cases} \quad (\text{A16})$$

Then we can separate the integration contour in Eq. (A14) into four parts and insert the appropriate asymptotic behavior in each piece. This gives us the following estimate for the contour integral:

$$\begin{aligned} \hat{W}_k &\approx \int_{-a}^{-\delta x^{1/2\nu_l}} \frac{d\delta z}{2\pi i} (\delta z + 1)^k w(\delta z) + \int_{-\delta x^{1/2\nu_l}}^0 \frac{d\delta z}{2\pi i} (\delta z + 1)^k w(\delta z) \\ &\quad + e^{2\pi i(1-\theta)} \int_0^{-\delta x^{1/2\nu_l}} \frac{d\delta z}{2\pi i} (\delta z + 1)^k w(\delta z) + e^{2\pi i(1-\theta)} \int_{-\delta x^{1/2\nu_l}}^{-a} \frac{d\delta z}{2\pi i} (\delta z + 1)^k w(\delta z) \sim \delta x^{1-\frac{\gamma}{2}}. \end{aligned} \quad (\text{A17})$$

Since $\gamma < 0$, we conclude that the first term in Eq. (A13) dominates $w^2(\delta x)$. Now we compare $w(\delta x) \sim \delta x^{1/2}$ with Eq. (11) and obtain another relation between exponents:

$$\frac{\nu_l(2 - \gamma) - 1}{2\nu_l} = \frac{1}{2}. \quad (\text{A18})$$

Finally, equations Eqs. (A12) and (A18) together determine both exponents:

$$\nu_l = 1 - \theta, \quad \gamma = -\frac{1}{2}. \quad (\text{A19})$$

For the case of percolation we have $n = 1$, $\theta = 1/3$, and the above result reduces to Eq. (14).

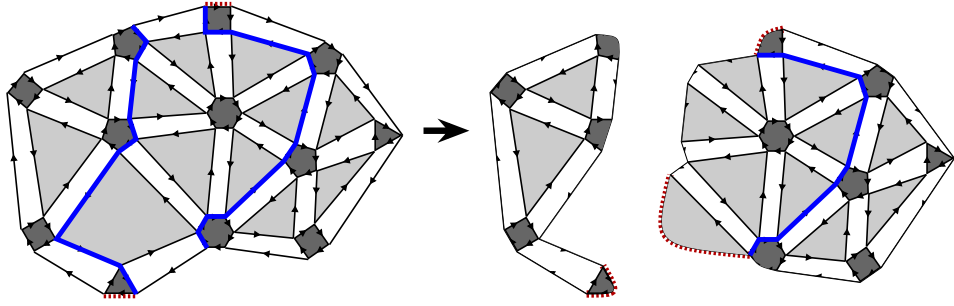


FIG. 8. An example of the splitting for a surface that contributes to the two leg correlation function.

Appendix B: L-leg operators

The boundary L -leg correlation functions (15) also satisfy LEs that can be derived from a combinatorial argument. The recursion relation in this case is

$$D_{ll'}^L(x) = x^{-1} \sum_p (W_{l+p}(x) D_{pl'}^{L-1}(x) + \dots). \quad (\text{B1})$$

To convert this into a functional LE, it is convenient to slightly modify the generating function in Eq. (16) by allowing the boundary fugacity to be different in the two parts separated by the marked points, namely

$$D^L(x, \zeta, \xi) = \sum_{ll'} \zeta^{-l-1} \xi^{-l'-1} D_{ll'}^L(x). \quad (\text{B2})$$

We will set the two boundary fugacities to be equal at the end of the calculation. In terms of this generating function Eq. (B1) translates to

$$D^L(\zeta, \xi) = \oint \frac{dz}{2\pi i} \frac{g_L(z) W(z) D^{L-1}(1/z, \xi)}{\zeta - z}, \quad (\text{B3})$$

where the functions $g_L(z)$ (which come from the many ways in which the two surfaces may be attached by the white faces adjacent to the marked sides) are smooth near the critical point $z = 1$. This is obtained in a similar way to the second contribution to the LE for $W(\zeta)$ but instead of cutting along a loop the surface is cut along the topmost “leg”. An example of this splitting for a surface that contributes to the 2-Leg correlation function is shown in Fig. 8.

Eq. (B3) implies that the singular behaviors of the L -leg correlator is related to the singular behavior of the one point function $W(\zeta)$ and the $(L-1)$ -leg correlator by

$$D^L(\zeta, \xi) \sim W(\zeta) D^{L-1}(1/\zeta, \xi). \quad (\text{B4})$$

Therefore, knowing the singular behavior of the zero leg correlator is enough to find the critical exponents. The zero leg correlator can be explicitly computed in terms of $W(\zeta)$ and is given by

$$D^0(x, \zeta, \xi) = \sum_{ll'} \zeta^{-l-1} \xi^{-l'-1} W_{l+l'} = -\frac{W(\zeta) - W(\xi)}{\zeta - \xi}. \quad (\text{B5})$$

Taking $\xi \rightarrow \zeta$ gives $D^0(x, \zeta, \zeta) = -\partial_\zeta W(\zeta)$ which, as we know from Eqs. (11) and (A12), behaves as $\delta \zeta^{-1/3}$. This result and the recursion relation in Eq. (B4) allows us to determine the critical behavior of the L -leg correlation function, which scales as

$$D^L(\zeta, \xi = \zeta) \sim \delta \zeta^{-1} W^{\lfloor L/2 \rfloor + 1}(\zeta) \dot{W}^{\lceil L/2 \rceil}(1/\zeta) \sim \delta \zeta^{2(L+1)/3 - 1}. \quad (\text{B6})$$

Comparing this to Eq. 18 gives $\tilde{\Delta}_L = L-1$. Furthermore, using Eq. (1) we get that the exponents on a non-fluctuating surface are $\tilde{\Delta}_L^{(0)} = L(L-1)/3$, which are the boundary exponents for the L -leg operators in bond percolation.